Biosensors and Bioelectronics 140 (2019) 111352

Contents lists available at ScienceDirect

Biosensors and Bioelectronics

journal homepage: www.elsevier.com/locate/bios

Immobilization-free photoelectrochemical aptasensor for environmental pollutants: Design, fabrication and mechanism

Caiqin Sun, Meichuan Liu*, Huanhuan Sun, Hanxing Lu, Guohua Zhao**

School of Chemical Science and Engineering, Shanghai Key Lab of Chemical Assessment and Sustainability, Tongji University, 1239 Siping Road, Shanghai, 200092, China

ARTICLE INFO

Keywords:
Atrazine
Graphene
TiO_2 nanotube
Immobilization-free
Photoelectrochemical aptasensor

ABSTRACT

Atrazine (ATZ) is one of the most widely used and highly toxic triazine herbicides in the world. Photoelectrochemical (PEC) method is an attractive and sensitive alternate for ATZ. However, for conventional PEC sensors, recognition elements usually need to immobilize on electrode surface, where a complex procedure is unavoidable and the reproducibility of sensors fabrication is usually poor. Therefore, we herein proposed a new and feasible strategy for developing a signal-on immobilization-free PEC aptasensor to ATZ. Aptamer for ATZ is combined with graphene to obtain APT-GN complex, serving as the recognition element in solution. TiO_2 nanotubes (NTs) electrode deposited with Au nanoparticles (NPs) is used as the substrate electrode. After further self-assembled with 1-Mercaptooctane (MCT), the photo-generated carriers transfer between the resultant electrode and the electrolyte will be blocked, leading to a signal-off of the photocurrent. But when sensing ATZ, aptamers on APT-GN will be grasped by ATZ, leaving free graphene to assemble onto MCT/Au NPs/TiO_2 NTs, which will largely "turn on" the photocurrent response of the substrate electrode due to the efficient carrier transport efficiency of graphene. Meanwhile, simultaneous addition of deoxyribonuclease I (DNase I) can bring about further cycling amplification of the signal enhancement. The as-designed PEC aptasensor exhibits a linear range from 50.0 fM to 0.3 nM with detection limit of 12.0 fM for ATZ. Since the reaction of recognition elements and targets ATZ occurs in homogeneous solution rather than on the photoelectrode surface, this PEC aptasensor exhibits advantages of high stability, anti-interference ability, reproducibility, and wide pH and ion strength feasibility range. A promising immobilization-free aptasensing platform has thus been provided not only for ATZ but also for other kinds of environmental pollutants.

1. Introduction

With the development of the industrialization in the world, the problem of environmental pollution has become increasingly serious. When environmental pollutants enter the living organism, they can cause biochemical changes in body fluids and tissues, interfere with or destroy the normal physiological functions of the body, and cause temporary or persistent pathological damage. Atrazine (2-chloro-4-ethylamino-6-isopropylamino-s-triazine, ATZ) is one of the most widely used highly toxic triazine herbicides in the world (Buser, 1990), which has serious disturbance effects on the endocrine system, central nervous system and immune system, and is a potential teratogen and carcinogen to humans (Hyer et al., 2001). In 1986, the maximum limit of ATZ and its degradation products was regulated to be 0.1 μg/L (0.1 ppb) in drinking water by European Union. In view of its great toxicity, it is great significant to establish methods for highly sensitive and accurate detecting of ATZ in environmental samples.

Photoelectrochemical (PEC) sensing, as a newly emerged analytical approach combining both optical and electrochemical techniques, not only owns the advantages of electrochemical analytic techniques, but also has a much more attractive ultrasensitivity capacity (Zhao et al., 2015). Since electronic detection devices, rather than sophisticated and expensive optical equipment, are adopted, PEC instrumentation demonstrates additional advantages of simplicity, low cost, and miniaturization (Osterloh, 2013). Due to such excellent properties, PEC sensing method has undergone tremendous development these years and has been applied in assaying typical environmental pollutants such as PCBs (Shi et al., 2016), Bisphenol A (Qiao et al., 2016; Lu et al., 2013), MC-LR (Liu and Yu et al., 2016a; Liu et al., 2017; Chen et al., 2012), antibiotics (Zhu et al., 2019; Zeng et al., 2019; Peng et al., 2018) and Hg^{2+} (Han et al., 2015) in the environment. ATZ is relatively difficult to be detected directly by simple electrochemical method due

* Corresponding author.
** Corresponding author.
E-mail addresses: liumc@tongji.edu.cn (M. Liu), g.zhao@tongji.edu.cn (G. Zhao).

https://doi.org/10.1016/j.bios.2019.111352
Received 21 March 2019; Received in revised form 16 May 2019; Accepted 24 May 2019
Available online 28 May 2019
0956-5663/

to its stable molecular structure. Therefore, PEC approach with ultra-high oxidation ability is a promising alternative for ATZ.

At the same time, an appropriate recognition element is important to obtain the selective sensing performance towards ATZ. In previous reports, the commonly used recognition elements for ATZ were molecularly imprinted polymer (MIP) (Kubo et al., 2008; Pardieu et al., 2009), enzyme (Jiang et al., 2006; Yu et al., 2010) and antibody (Wang et al., 2017; Bhardwaj et al., 2015). However, the inherent disadvantages of these recognition elements, for instance, molecularly imprinted polymers were hindered signal transmission, while enzymes and antibodies were easily inactivated, largely limit their applications. Aptamer, termed as "artificial antibodies" that are synthetic single stranded DNA or RNA sequences which can bind their targets with high affinity and specificity (Ellington et al., 1990), has recently been used to build impedimetric aptasensor to ATZ (Madianos et al., 2018), and good selectivity has been achieved towards ATZ with aptasensor.

However, for most reported aptasensors, the recognition elements aptamers need to immobilize onto the electrode surfaces. As we know, some obvious limitations for such immobilization-based sensors (Hou et al., 2018) are unavoidable, including that: (i) The immobilization operations are usually complicated and time-consuming, and it is rather hard to fabricate sensors without differences. (ii) The modification conditions of the recognition probes on the surface need to be carefully optimized to obtain proper density and orientation, otherwise the binding efficiency between the target and the probe might be damaged, because the steric effect of the surface may cause changes in the geometric conformation of the probe. (iii) Due to the limited loading of the surface recognition elements of the electrode, the target substance is easy to achieve saturated adsorption, which directly affects the detection sensitivity of the sensor. (iv) Immobilization-based sensors are normally difficult to regenerate once a target substance recognition has occurred because of the residue of target material or the change of the micro-environment of the sensor itself. (v) In complex detection system, the stability of the recognition molecules is also a great challenge, especially in the PEC analysis. The recognition element structure is easy to change and even loses its specific recognition ability and may produce interference signals under light condition. Therefore, how to design an immobilization-free PEC aptasensor towards environmental pollutants, of which the aptamers do not need to immobilize onto the photoanodes, is of great interest and is a challenging topic.

Since the Hsing and co-workers' work (Xuan et al., 2012) of DNA sensing based on solution-phase electrochemical molecular beacon was reported, the possible strategies to realize immobilization-free electrochemical (EC) analysis have aroused more and more concern and quite a number of interesting ideas (Yan et al., 2013; Liu and Ke et al., 2019a; Liu and Sun et al., 2019b; Liu et al., 2014; Hou et al., 2015; Tan et al., 2015; Fu et al., 2016) have been proposed. However, there are few reports on immobilization-free PEC analysis, in which photoactive organic molecules modified at the end of single-stranded DNA strands, such as the organic dye methylene blue (MB) or toluidine blue (TB) (Hou et al., 2018; Ge et al., 2016), are used as signal molecules to realize signal on or off. And photoactive organic molecules modified DNA may be unstable and much more expensive than unmodified ones.

Recently, we proposed a signal-on immobilization-free EC aptasensor towards microcystin-LR (MC-LR) based on synergistic signal amplification strategy with graphene, DNase I enzyme and Au nanoparticles (Liu and Sun et al., 2019b), in which the signal amplification reaction took place in solution, and the naked graphene with excellent conductivity was assembled onto the surface of substrate electrode to restore electron transfer (eT) channel blocked by alkylate thiol instead of dye molecules. Inspired by the idea that graphene is also an excellent promoter and conductor for photogenerated carriers, we wonder whether the proposed electrochemical signal amplification strategy can be applied to photoelectric sensing to build an immobilization-free PEC aptasensor system to pollutants that does not need to modify aptamers with photoactive probes.

Therefore, in this work, we developed an immobilization-free synergistic signal amplified method based on aptamer-graphene (APT-GN) complex and deoxyribonuclease I (DNase I) for sensitively detecting ATZ for the first time. The TiO_2 NTs electrode modified by Au nanoparticles (NPs) (Au NPs/TiO_2 NTs) was used as the substrate electrode, in which Au NPs are not only to improve PEC performance of TiO_2 NTs significantly but also to provide large surface area for self-assembled monolayer (SAM) loading. Alkylate thiol 1-Mercaptooctane (MCT) was chosen to serve as the block agent, which could self-assembled onto Au NPs/TiO_2 NTs surface via Au–S covalent bond and block the carriers transfer between electrode and electrolyte in an appropriate degree. Graphene was used as a "molecular switch" for photoelectric signals (Song et al., 2016), which worked when ATZ react with the APT-GN complex to form ATZ-APT complex and leave "naked" graphene. Moreover, simultaneous addition of DNase I could lead to cycling amplification of the signal enhanced MCT/Au NPs/TiO_2 NTs electrode. The proposed PEC aptasensor towards ATZ exhibits outstanding sensitivity, high selectivity, and good stability. This immobilization-free sensing stratagem is very promising not only to ATZ but also to other kinds of targets including different contaminants in evironmental samples.

2. Experimental

2.1. Reagents and apparatus

The single-strand DNA (ssDNA) aptamer of atrazine (ATZ) was chosen according to the prior reported literature (Williams et al., 2014) with the sequence of 5′-TGT-ACC-GTC-TGA-GCG-ATT-CGT-ACG-AAC-GGC-TTT-GTA-CTG-TTT-GCA-CTG-GCG-GAT-TTA-GCC-AGT-CAG-TGT-TAA-GGA-GTG-C-3′, and was purchased from Shanghai Sangon Biotechnology Co. Ltd. (Shanghai, China) without any modification. Other reagents and apparatus information is listed in supporting information (SI, S1) in detailed.

2.2. Design and fabrication of aptamer-graphene (APT-GN) complex and MCT/Au NPs/TiO_2 NTs electrode

As shown in Scheme 1, to construct the ATZ PEC aptasensing system, the APT-GN complex and the substrate electrode were designed and prepared as follows.

APT-GN complex was prepared by combining well-dispersed graphene with anti-ATZ aptamers under ultrasound condition in ice bath (Liu et al., 2019a, b). Briefly, graphene was added to DI water and sonicated for 3 h to obtain homogeneous graphene dispersion with a concentration of 0.15 mg/mL. Then, 130 μL of the aqueous graphene dispersion was added to anti-ATZ aptamers, and the mixture was incubated in ice bath under ultrasound condition for 3 h. Due to the intrinsic giant π-conjunction and hydrophobic properties of graphene, aptamers can be adsorbed onto graphene through π-π stacking interaction and hydrophobic interaction (Lu et al., 2009). In order to remove unmodified graphene and get fully integrate aptamer with graphene, while reducing system background current, the obtained suspension was then centrifuged at 2000 rpm for 5 min to remove the large pieces of graphene. 10 μM APT-GN complex dispersion was thus obtained.

Ti foils were polished to a smooth surface before use, and were cleaned via ultrasonication in acetone, ethanol and DI water successively, followed by drying in N_2 flow. Electrochemical anodization was performed using a DC power supply in a two-electrode configuration with the Ti foil as the anode and a platinum foil as the cathode. Anodization was carried out at 0 °C and 60 V for 3 h in electrolytes including ethylene glycol and glycerol (1:3, v/v) with 3 M H_2O and 0.54 M NH_4F (Lee et al., 2013), and then the as-grown nanotube layer was ultrasonically removed in DI water. After that, a second anodization was taken to the Ti foil at 60 V for 1 h, followed by ultrasonically removing the as-grown nanotube layer again in DI water. Finally a third

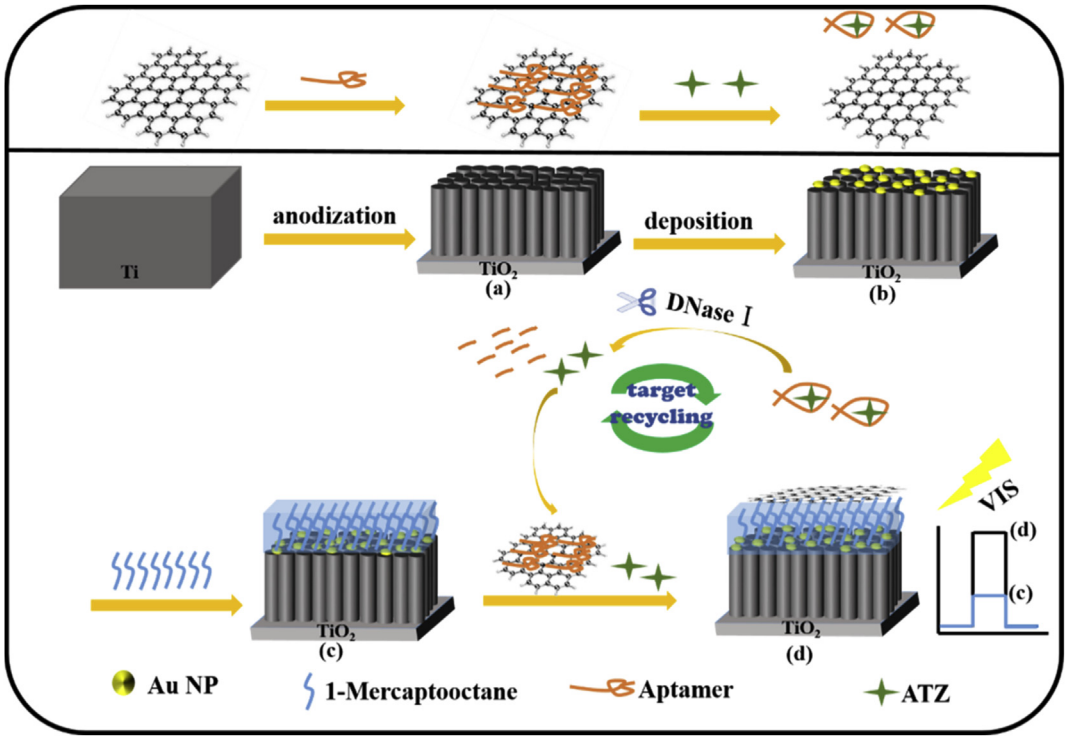

Scheme 1. Illustration for the construction of the immobilization-free PEC aptasensor.

anodization was taken to the Ti foil at 20 V for 5 min. After the anodization process, the samples were rinsed with water and then dried in air, followed by heat-treating at 550 °C for 180 min in air with a heating rate of 5 °C/min. TiO_2 nanotubes (NTs) were thus obtained.

Au NPs were deposited onto TiO_2 NTs by photocatalytic reduction method (Zhang et al., 2013). The TiO_2 NTs were first immersed in a 0.3 mM aqueous solution of $HAuCl_4$ for 24 h, and then the TiO_2 NTs absorbed Au^{3+} was irradiated in this solution with a 300 W Xe lamp for 1 h to reduce Au^{3+} to Au^0 by photocatalysis at the expense of water oxidation. The $HAuCl_4$ concentration and the irradiation time was optimized (as shown in SI, Fig. S1 and Fig. S2).

The as-prepared Au NPs/TiO_2 NTs electrode was then immersed in 40 mM MCT overnight to formed MCT self-assembled molecular (SAM) layer on the surface through Au–S bonds. Thus, MCT/Au NPs/TiO_2 NTs electrode was obtained.

2.3. Photoelectrochemical sensing procedure of ATZ

To sense ATZ, MCT/Au NPs/TiO_2 NTs electrode was incubated with 20 μL Tris-HCl buffer, 10 μL APT-GN complex, 4 μL DNase I, and 6 μL target ATZ of different concentrations, denoted as sensing system (sensing sys), at 30 °C for 1 h, wherein the incubation time was optimized by *I-t* method (as shown in Fig. S3). After the incubation, the electrode was washed with DI water and ethanol to remove the uncombined substance and then dried in N_2. For calculating the dose-response turn-on signal for ATZ, the photocurrent of MCT/Au NPs/TiO_2 NTs electrode before and after incubation with the sensing sys containing different concentrations of ATZ were measured by *I-t* method, respectively. According to the turn-on signal of the electrode, estimated by their photocurrent change, the quantitative determination of ATZ could be realized. Unless otherwise specified, the electrolyte solution used in the *I-t* method was 0.1 M PBS (pH = 7.4), and the applied bias voltage was +0.5 V according to the photoelectric conversion efficiency (SI, Fig. S4).

3. Results and discussion

3.1. The design, fabrication and characterization of ATZ aptasensor system

The construction process of ATZ PEC aptasensor is illustrated in Scheme 1. APT-GN complex was prepared via π-π stacking reaction between the graphene hexagonal cells and the nucleobases of aptamers (Lu et al., 2009; Eissa et al., 2014). Reduction of Au^{3+} to Au NPs by photoreduction occurred on the surface of TiO_2 NTs. Then it was immersed in MCT ethanol solution overnight to form MCT SAM layer via Au–S covalently bonded on Au NPs/TiO_2 NTs. Due to the strong hydrophobic effect of MCT, which could hinder effective photogenerated carriers transfer between the MCT/Au NPs/TiO_2 NTs electrode surface and the electrolyte, the probability of electrons and holes combination were increased. As a result, a drastic decrease of the photocurrent signal would be observed.

However, when the MCT/Au NPs/TiO_2 NTs electrode incubated with APT-GN complex, target ATZ, and DNase I, the aptamer would be detached from the surface of graphene due to the specific recognition reaction between ATZ and aptamer, and the “naked” graphene would be exposed, which would assemble to the surface of the MCT/Au NPs/TiO_2 NTs electrode due to the hydrophobic interaction and π-conjunction. Owing to the excellent carriers' conductivity of graphene, the photogenerated electrons and holes “channel” blocked by MCT SAM layer can be restored, and the photoelectrical signal will be turned on. It has been reported that DNase I is capable of cleaving an aptamer that binds to a target molecules at a specific site, allowing long-chain aptamer to be cleaved into DNA fragments and release free target molecules, but can't shear the aptamer that bound to graphene (Sun et al., 2017). Therefore, in the presence of DNase I, the obtained ATZ-APT complex can be cleaved, and then ATZ will be released, which can reattack other aptamers on graphene. Following that, the cycle resumes, resulting in the successive release of ATZ, leading to a further amplification of PEC signal. Therefore the dose-response curve of ATZ and the photocurrent signal can be obtained.

Fig. 1A presents a top view SEM image of TiO_2 NTs, indicating that

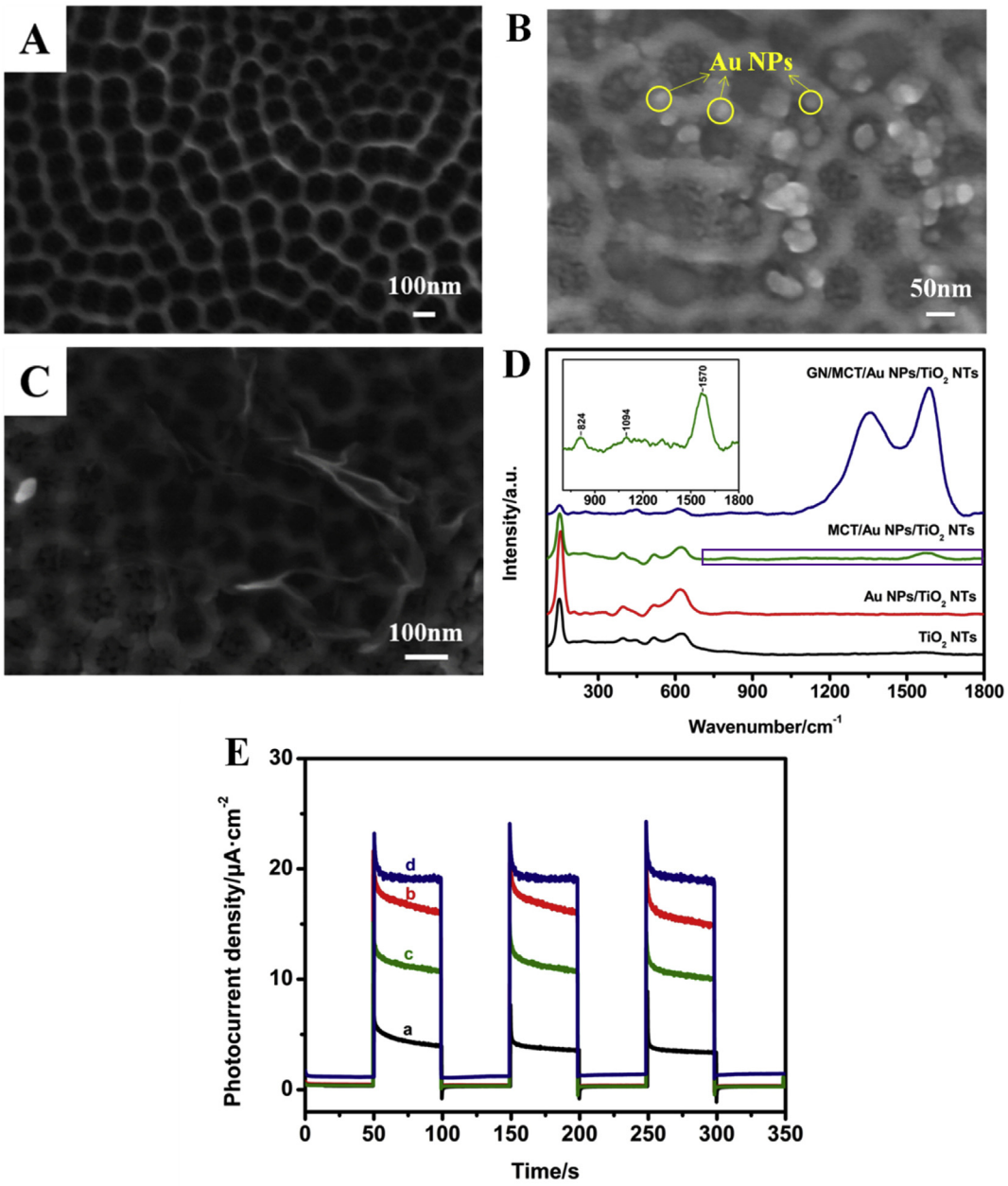

Fig. 1. SEM images of TiO_2 NTs(A), Au NPs/TiO_2 NTs(B), and GN/MCT/Au NPs/TiO_2 NTs (C); Raman spectrum (D) and *I-t* response in 0.1 M PBS (pH = 7.4) with visible light illumination (E) of diverse electrodes. The inset in Fig. 1D is a partial enlargement of the Raman spectrum of MCT/Au NPs/TiO_2 NTs electrode.

the resultant TiO_2 NTs consist of a periodic upright ordered array of nanotubes that can provide large specific surface for Au NPs deposition. The nanotube diameter and wall thickness of TiO_2 NTs are ca. 100 nm and ca. 20 nm, respectively, with regularly round-shaped and smooth open structure which can facilitate modification of Au NPs. The top-view SEM image of the prepared Au NPs/TiO_2 NTs is shown in Fig. 1B, which clearly exhibits the Au NPs are well-dispersed on TiO_2 NTs with average size of 15–30 nm. After the loading of Au NPs, the nanotube structure of TiO_2 NTs is still well maintained. The energy dispersive X-ray spectroscopy (EDS) spectrum (Fig. S5) and Mapping spectrum (Fig. S6) of the Au NPs/TiO_2 NTs present another evidence of the successful Au deposition. The XRD patterns (Fig. S7) of TiO_2 NTs show dominant anatase phase with preferential orientation of (101). The dominant Au peaks in the XRD pattern of the Au NPs/TiO_2 NTs could be assigned to the (111) plane and (220) plane. According to Fig. 1C, after interaction with graphene, numerous microscale layers of graphene nanosheets can be seen lying on MCT/Au NPs/TiO_2 NTs surface uniformly and stably by hydrophobic interaction and π-conjunction between graphene and MCT. The graphene neither completely covers the surface of MCT/Au NPs/TiO_2 NTs nor destructs their tubular structure, which is of great benefit to restore the photocatalytic properties of MCT/Au NPs/TiO_2 NTs. It might also be attributed to the fact that graphene with its two-dimensional (2D) planar structure bears a giant π-π conjunction system, which can reopen the carriers channel between the electrode and the electrolyte.

Since Raman spectroscopy is sensitive to the characteristic peaks of reactive species, Raman spectroscopy is further used to prove the successful preparation of the aptasensor. As shown in Fig. 1D, all electrodes show characteristic peaks of TiO_2 NTs at 148, 200, 395, 516 and 627 cm^{-1}, which are attributed to Raman active vibration of E_g, E_g, B_{1g}, B_{1g} and E_g of anatase TiO_2, respectively (Soejima et al., 2013). When Au NPs are deposited onto TiO_2 NTs, no new Raman scattering peaks

appear, while the intensity of the characteristic peaks attributing to anatase TiO_2 increased due to the Raman enhancement of Au NPs (red line). After self-assembly of MCT onto Au NPs/TiO_2 NTs, several characteristic Raman scattering peaks of MCT appear (green line). The peak at 824 cm^{-1} corresponds to the out of-plane bending vibration of C–H, while that at 1094 cm^{-1} corresponds to the C–S stretching vibration, and peaks at 1570 cm^{-1} corresponds to non-symmetry stretching vibration of C–C (Joo et al., 1987) (as shown in the inset in Fig. 1D). All these new peaks prove the successful growth of MCT on the electrode surface. However, it is still not clear why the peak intensity at 1570 cm^{-1} is significantly stronger than those at 803 cm^{-1} and 1060 cm^{-1}. After incubation with the sensing system, the Raman spectra of the resulting electrodes showed two characteristic peaks at 1356 and 1584 cm^{-1}, corresponding to the D and G peaks of graphene, respectively (blue line) (Park et al., 2017). This gave direct evidence for the successful combination of graphene onto MCT/Au NPs/TiO_2 NTs after incubation with ATZ, APT-GN complex and DNase I.

3.2. Sensing mechanism of ATZ PEC aptasensor

In order to optimize the bias voltage, a linear sweep voltammetry (LSV) test is conducted on Au NPs/TiO_2 NTs electrode and then the photoelectric conversion efficiency of the electrode at different potentials is calculated. Results show that the photoelectric conversion efficiency of the electrode is different under different bias voltages, and reaches the maximum at +0.5 V (detailed results and calculations are shown in SI, Fig. S4). Therefore, a bias of +0.5 V is applied throughout the subsquent *I-t* experiments.

The photocurrent responses for different electrodes upon irradiation with visible light were displayed in Fig. 1E. A weak photocurrent response (ca.3.78 μA·cm^{-2}, black line, curve a) was observed for TiO_2 NTs electrode at 0.5 V. It may be due to the fact that TiO_2 NTs array with periodic upright order structure can improve the absorption of visible light by increase the refraction and reflection of light in nanotubes (Wu et al., 2015). Compared to TiO_2 NTs, the photocurrent density was greatly improved to 16.75 μA·cm^{-2} for Au NPs/TiO_2 NTs electrode (red line, curve a), more than 4.4 times that of the former. This was attributed to the fact that Au NPs not only can extend the absorption range of the modified TiO_2 NTs electrode due to its surface plasmon resonance (SPR), but also can suppress the charge recombination by forming a hetero-junction between Au and TiO_2. After self-assembly of MCT, the photocurrent response decreased to 11.23 μA·cm^{-2} under the same condition (green line, curve c), indicating that the MCT SAM layer greatly inhibits the heterogeneous carriers transfer. However, it increased to 19.31 μA·cm^{-2} for GN/MCT/Au NPs/TiO_2 NTs electrode (blue line, curve d). That is obviously caused by the loading of "naked" graphene onto MCT/Au NPs/TiO_2 NTs surface and hence opening the carriers transfer tunnel of the electrode. Ultraviolet visible (UV–vis) diffuse reflectance spectroscopy (DRS) can more intuitively evaluate the absorption properties of different electrodes. Results show that the modification of naked graphene on MCT/Au NPs/TiO_2 NTs electrode can significantly enhance the light absorption capacity reduced by MCT (Fig. S8).

The feasibility of the proposed PEC aptasensor for ATZ was investigated by carrying out PEC measurements under different conditions. As shown in Fig. 2, the photocurrent density for MCT/Au NPs/TiO_2 NTs electrode in 0.1 M PBS (pH = 7.4) was ca. 11.23 μA·cm^{-2} (green line, curve a). While for MCT/Au NPs/TiO_2 NTs electrode after incubation in sensing system without ATZ (only containing APT-GN complex and DNase I), the photocurrent density in PBS remained almost unchanged (11.26 μA·cm^{-2}, purple line, curve b), revealing that DNase I cannot cleave the aptamer in the APT-GN complex or generate the signal amplification probe graphene. Our previous reports have also proved this conclusion (Liu and Ke et al., 2019a; Liu and Sun et al., 2019b). However, it is noticeable that after incubation in sensing system with 5.0 nM ATZ, the photocurrent density increased to 19.31 μA·cm^{-2} (blue line, curve c). It illustrates that the graphene on APT-GN complex can not assemble to the MCT/Au NPs/TiO_2 NTs electrode surface; while ATZ can bind to the aptamer of APT-GN complex with high selectivity, leading to the produce of "naked" graphene to restore the "channel" of photogenerated carriers' transfer.

We further evaluated whether DNase I can trigger target recycling. As shown in Fig. 2B, compared to the photocurrent density for MCT/Au NPs/TiO_2 NTs before incutation (green line, curve a), it increased to 15.21 μA·cm^{-2} for the electrode incubated in sensing system without DNase I (i.e., only containing Tris-HCl buffer, APT-GN complex, 5.0 nM ATZ) (orange line, curve b′). The change of photocurrent ($\Delta j_{b'\text{-}a} = j_{b'} - j_a$, the same below) is calculated to 3.98 μA·cm^{-2}, which is only 49.3% of the value for $\Delta j_{c\text{-}a}$ (8.08 μA·cm^{-2}) that corresponds to the photocurrents for the electrode after incubation in sensing system with DNase I (Fig. 2D). This is logically ascribed to the fact that aptamers bound with ATZ can be cleaved by the DNase I, releasing ATZ which can reattack other aptamers on APT-GN complex. Following that, the cycle starts anew, leading to the successive release of ATZ and further graphene, resulting in the greatly increase of PEC signal.

To understand the important role of graphene in the sensing system, PEC behavior of MCT/Au NPs/TiO_2 NTs after incubating in a same sensing system with aptamer instead of APT-GN complex (i.e., only containing Tris-HCl buffer, aptamer, DNase I, and 5.0 nM ATZ) was investigated (Fig. 2C, pink line, curve b″). In comparison, the response is almost the same to that for MCT/Au NPs/TiO_2 NTs before incubation. The $\Delta j_{b''\text{-}a}$ is calculated to only 0.54 μA·cm^{-2}. That means although the aptamer can recognize ATZ and combine with it, but since there's no graphene to assemble onto MCT/Au NPs/TiO_2 NTs surface, no turn-on signal can be observed. On the contrary, the large value of $\Delta j_{c\text{-}a}$ (8.08 μA·cm^{-2}) for MCT/Au NPs/TiO_2 NTs electrode after incubating in the same sensing system with APT-GN complex is clearly attributed to the self-assemble of graphene to the MCT/Au NPs/TiO_2 NTs electrode surface to restore the "channel" of carriers transfer that hindered by MCT molecular film.

According to the above experiments, a possible sensing mechanism is proposed (Fig. 3). When Au NPs/TiO_2 NTs electrode is subjected to the visible light irradiation, due to surface plasmon resonance, the Au NPs generate hot electron-hole pairs (Zhao et al., 2017). The hot electrons injecting to TiO_2 conduction band (CB) is accomplished by overcoming Schottky barrier, which is generated due to the large work function of gold and it can effectively suppress the recombination of electrons and holes. Subsequently, the CB electrons of TiO_2 tend to transfer into external circuit. After MCT SAM modification, the combination probability of electrons and holes increases and the carriers transfer channel is properly blocked due to MCT's hydrophobic and insulating properties. When senging ATZ, graphene can be released from the APT-GN complex, and the obtained "naked" graphene which is equipped with high density edge-plane-like defects and excellent carriers' conductivity, is assembled onto the electrode surface. Then the remaining holes tend to transfer to graphene from Au NPs and the hot electrons transfer to external circuit. As a result, the carriers transfer "channel" on electrode surface that hindered by MCT molecular film can be restored. Mott-Schottky plots (Fig. S9) have been studied and the potential mechanism of photoactivity enhancement of the Au NPs/TiO_2 NPs under visible light irradiation has also been discussed in SI (S2) accordingly.

3.3. Sensing performance of ATZ PEC aptasensor system

The photocurrent of MCT/Au NPs/TiO_2 NTs electrode is measured by *I-t* method after incubation in the sensing system with different concentrations of ATZ. Fig. 4A reveals an obvious concentration-dependent response of the photocurrent density towards a series of different concentration ATZ.

It can be seen that comparing to the photocurrent for sensing system without ATZ, the photocurrent increases significantly even for ATZ with

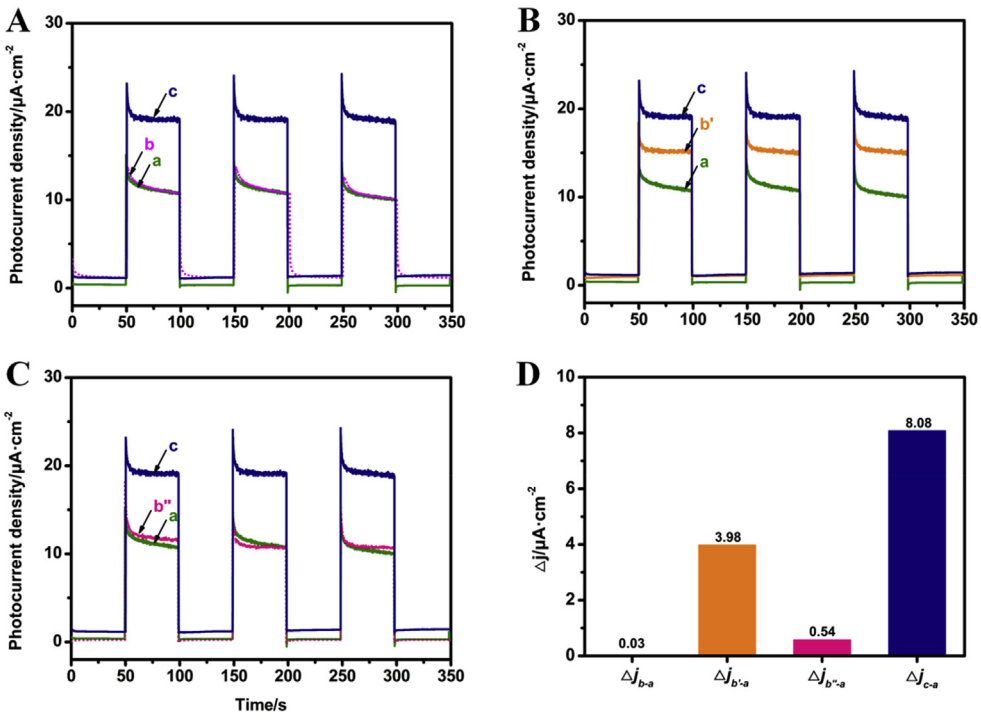

Fig. 2. *I-t* responses of MCT/Au NPs/TiO_2 NTs in 0.1 M PBS (pH = 7.4) under visible light illumination (A, B, C) before incubation (a) and after incubation (b, b′, b″, c) in sensing system containing APT-GN complex, 5.0 nM ATZ, DNase I (c) or sensing system without ATZ (b), without DNase I (b′), without APT-GN complex while with aptamers instead (b″); Photocurrent density change Δ*j* (D) calculated from A, B, C, where $\Delta j_{b\text{-}a} = j_b\text{-}j_a$, $\Delta j_{b'\text{-}a} = j_{b'}\text{-}j_a$, $\Delta j_{b''\text{-}a} = j_{b''}\text{-}j_a$ and $\Delta j_{c\text{-}a} = j_c\text{-}j_a$.

concentration as low as 50.0 fM. As the concentration of ATZ further increases, the photocurrent increases accordingly (Fig. 4A). It can be reasonably considered that the formation of ATZ-aptamer causes the exposed graphene assembled onto MCT/Au NPs/TiO_2 NTs electrode and restores the path of carriers transfer. We calculated the increase in photocurrent density caused by ATZ in detail according to the following formula:

$$\Delta j = (j_{A(on)} - j_{A(off)})_{ATZ} - \left(j_{A(on)} - j_{A(off)}\right)_0$$

Where $j_{A(on)}$ is the average value of the current under light condition, $j_{A(off)}$ is the average value of the current under dark condition. The subscript character $(\,)_{ATZ}$ and $(\,)_0$ represent the photocurrent density for sensing system with and without ATZ, respectively. The curve of Δj corresponding to ATZ concentration is plotted (Fig. 4B), in which the Δj increases rapidly from 50.0 fM to 0.3 nM, while slows down from 0.3 nM to 1.0 nM, and the change of photocurrent density is relatively small from 1.0 nM to 5.0 nM. The linear curve of photocurrent corresponding to the logarithm of ATZ concentration is further plotted (inset of Fig. 4B) and it is found that there is a good linearity between Δj and $\lg C_{ATZ}$ in the range from 50.0 fM to 0.3 nM ($R^2 = 0.9938$) (the inset of Fig. 4B). At the same time, the limit of detection was estimated to be 12.0 fM ($S/N = 3$), which is more sensitive than those obtained by HPLC (Barchanska et al., 2012), GC-MS (Guan et al., 2017), SERS (Rubira et al., 2014), impedimetric aptasensor (Madianos et al., 2018), Immunosensor (Bhardwaj et al., 2015), QCM sensor (Gupta et al., 2015), MIP EC sensor (Li et al., 2015), Fluorescence (Liu and Li et al., 2016b), etc. The detailed detection linear range and detection limitation of the relating work were summarized in SI (S3, Table S1).

3.4. Superior selectivity, stability and reproducibility of ATZ PEC aptasensor

In order to evaluate the selectivity of the immobilization-free ATZ PEC aptasensor, experiments are performed by measuring changes in photocurrent density of aptasensor after incubation with 5.0 pM ATZ together with 100-fold concentration contaminants mixture, respectively. There are some interfering substances with similar structures that may coexist in real water samples, such as paraquat, glyphosate, trichlorfon, acetamiprid and clofentezine (their structural formulas are shown in the inset of Fig. 5A), selected as potential disruptors. The selectivity is evaluated by estimating the relative photocurrent density ratio, *R*(%), which is calculated by the following equation:

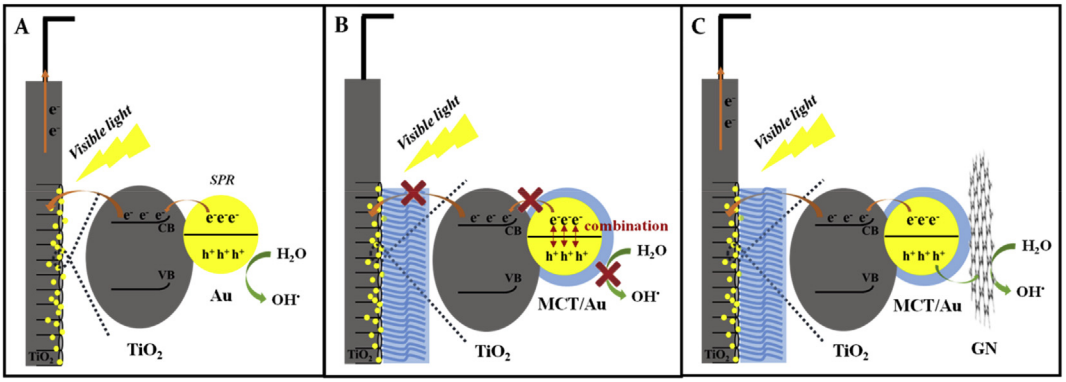

Fig. 3. Schematics of carriers transfer under visible light at Au NPs/TiO_2 NTs (A), MCT/Au NPs/TiO_2 NTs (B) and GN/MCT/Au NPs/TiO_2 NTs (C) interface.

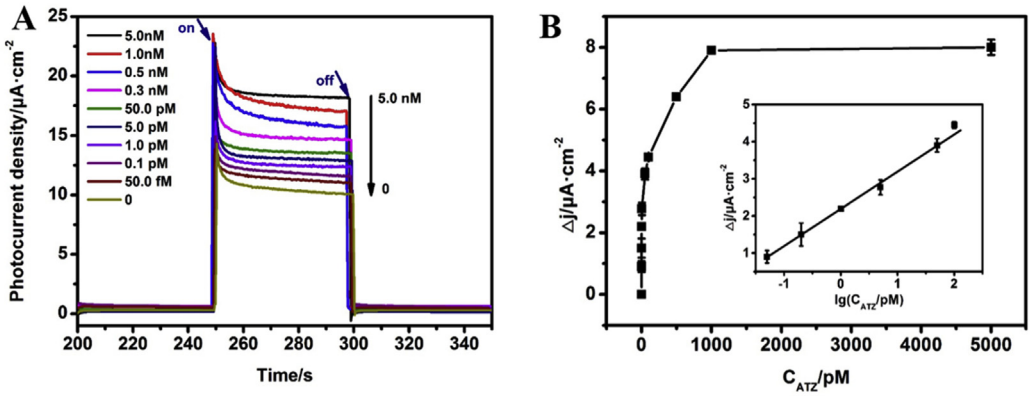

Fig. 4. (A) The photocurrent response of the PEC aptasensor after incubation in sensing system containing ATZ from 0 to 5.0 nM. (B)The relationship between the response current and ATZ concentration, and the inset is the liner calibration curve of the current and the logarithm of ATZ concentration (error bars calculated by $n = 3$).

$$R(\%) = (j_{ATZ+C} - j_{ATZ})/j_{ATZ} \times 100\%$$

where j_{ATZ} is the photocurrent density for 5.0 pM ATZ, j_{ATZ+C} is the photocurrent density for mixture of 5.0 pM ATZ and 100-fold concentration contaminant. The relative photocurrent density ratio of 5.0 pM ATZ is set to be 100%. Results show that the relative photocurrent density ratio is less than 5% after addition of 100-fold concentration of the interferents including paraquat and acetamiprid. For 100-fold concentration of glyphosate, trichlorfon and clofentezine, the relative photocurrent density ratio is less than 10% (Fig. 5A). Besides, the R(%) values for the aptasensor's selectivity against a common proteins, bovine serum albumin (BSA), and a commonly existing pollutant in real water sample with large molecular weight, humic acid, are still less than 7% under the same conditions. All results indicate that the aptasensor has high selectivity and affinity for ATZ. It can be attributed to the use of aptamer as recognition element for PEC aptasensor, which can bind target ATZ with high binding affinity and specificity, confirmed by circular dichroism (CD) spectrum.

The stability, another important factor of the ATZ PEC aptasensor, is evaluated by repeatedly turning the excitation light on and off and continuously recording the time-based photocurrent response (Fig. 5B). It is observed that the photocurrent is very stable and the relative standard deviation (RSD) was only 5.0% after 10 cycles, which gives the clear proof that the constructed ATZ PEC aptasensor having outstanding stability.

Moreover, since the water samples are often acid or alkaline and with high concentrations of ions in the actual environment, the effects of pH and Na^+ ionic strength of ATZ-containing samples on the proposed immobilization-free PEC aptasensor are investigated by the same *I-t* method to detect ATZ samples (c_{ATZ} = 5.0 nM) in electrolytes with different pH (pH = 1–13) and different concentrations of Na^+

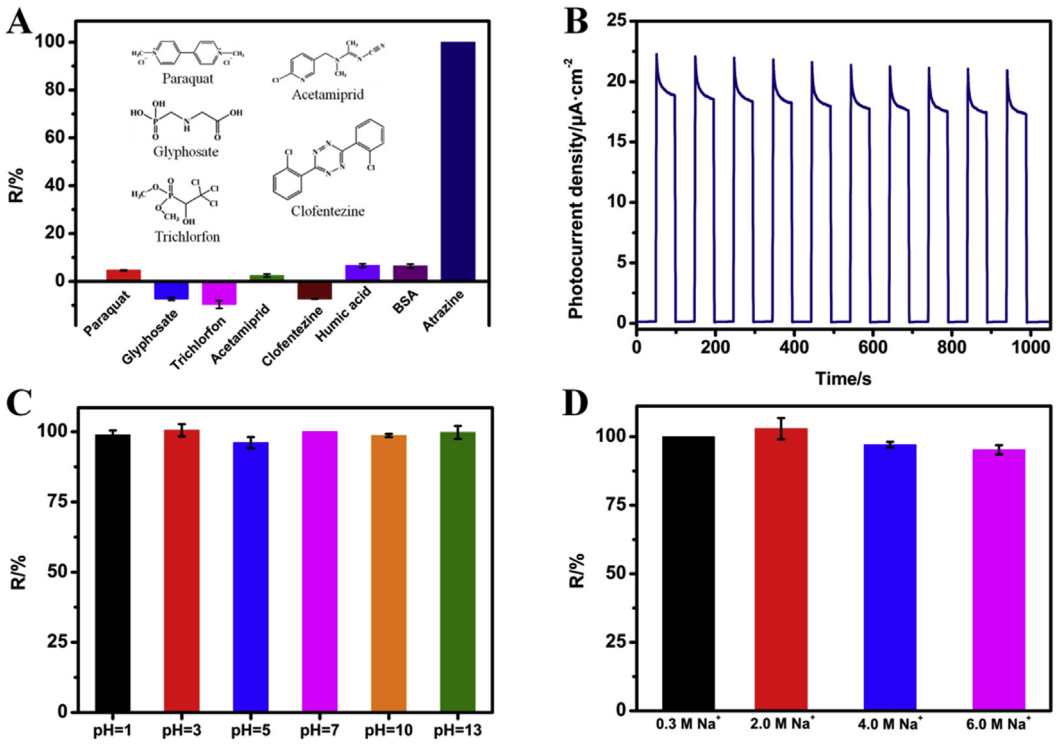

Fig. 5. (A) The selectivity test of the ATZ PEC aptasensor, where the ratio of the response for ATZ (R%) is set to be 100%. (B) Stability of photocurrent of the aptasensor after incubation in sensing system containing 5.0 nM ATZ, and effects of pH (C) and Na^+ ionic strength (D) of ATZ-containing samples (c_{ATZ} = 5.0 nM) on the immobilization-free ATZ PEC aptasensor, where the ratio of the response for ATZ (R%) in pH 7 and 0.01 M Na^+ is set to be 100%, respectively.

(2.0–6.0 M), respectively. Results (as shown in Fig. 5C and D) shows that the photocurrent density of the aptasensor remains 98.9% and 99.7% even for ATZ under pH = 1 and pH = 13. And in the electrolyte with increasing Na^+ concentration, the photocurrent density of the electrode is hardly reduced, even in an electrolyte containing 6.0 M Na^+, the photocurrent is only reduced by 4.8%. The wide pH and ion strength feasibility range of the present PEC aptasensor might be reasonably owing to the distinct immobilization-free characteristics of the sensing platform. One the one hand, when sensing ATZ samples, the MCT/Au NPs/TiO_2 NTs electrode is first incubated with sensing system, which contains 20 μL Tris-HCl buffer, 10 μL APT-GN complex, 4 μL DNase I, and 6 μL target ATZ of different concentrations for 1 h. That's to say, the volume of ATZ in the sensing system is relatively small, and there's Tris-HCl buffer present at the same time. So the activity of DNase I will not be affected by extreme pH or strong ion strength of the ATZ samples during incubation. On the other hand, after incubation for 1 h, the electrode is gently rinsed with DI water to remove unbound substance. Since graphene, the product of the specific reaction of ATZ and APT, can bind to MCT, only graphene remains on the surface of MCT/Au NPs/TiO_2 NTs electrode. And the further *I-t* test is performed on the obtained electrode after incubation. Since there're no biomolecules of aptamers or DNase I on the electrode any more, the photocurrent performance will not affected by the pH or ion strength conditions. Results show that the photocurrent response is almost unchanged even under pH = 1 or pH = 13 conditions, or even in an electrolyte containing 6.0 M Na^+. Therefore, the present immobilization-free aptasensor system can effectively avoid the interference of external extreme pH and ion strength factors on DNase I and the aptamer.

In addition, the reproducibility of the PEC aptasensor is investigated by evaluating the photoelectric response of several independently prepared MCT/Au NPs/TiO_2 NTs electrodes after incubation with the sensing system containing 5.0 nM ATZ. According to the *I-t* results, the RSD of the photocurrents of the six electrodes is calculated to be 3.9%, which means that the proposed immobilization-free aptasensor has good reproducibility. The results reveal that the immobilization-free aptasensor has great application potential. It is mainly related to the aptamer loaded on graphene, and then firm loading of naked graphene nanosheets on the MCT functionalized electrode surface, instead of modifying the aptamer directly on the electrode surface.

3.5. Real water sample analysis

A preliminary application of the proposed PEC aptasensor in real samples is performed through the measurement of one living community pond to evaluate the analytical reliability and application potential of the proposed method, and the results are summarized in SI (S3, Table S2). Results show that recoveries of 103.1%–113.0% are achieved for the water sample with standard addition method. The related standard deviation (RSD) is all less than 8% (n = 3), indicating that the proposed sensing platform is promising in the real sample monitoring.

4. Conclusions

In summary, an immobilization-free PEC aptasensor system has been successfully proposed for ATZ based on a novel synergistic signal amplification strategy. Compare to traditional immobilization-based PEC aptasensors, two significant advantages of our work should be emphasized. First, the aptamer's recognition response to ATZ is designed to occur in solution, avoiding the inherent limitations of immobilized-based PEC aptasensor while achieving high selectivity. Second, we use graphene as a signal amplifying molecule rather than modifying the photoactive material on the recognition element, exhibiting more sensitive, convinient, and cost-effective. The limit of the detection for ATZ by the present immobilization-free PEC aptasensor is estimated to be as low as 12.0 fM and the linear range is from 50.0 fM to 0.3 nM. At the same time, this immobilization-free PEC aptasensor exhibits good stability and selectivity and has been successfully applied to the analysis of real samples. In particular, this immobilization-free sensing method is not only promising suitable for ATZ but also significant for other small polutants to detect. Nevertheless, the in-depth and detailed molecular mechanism of synergistic signal amplification and the switching effects of photogenic electron-hole transferring channels are still not fully understood. And we will focus on the relating studies in the future.

CRediT authorship contribution statement

Caiqin Sun: Conceptualization, Data curation, Investigation, Methodology, Formal analysis, Validation, Visualization, Writing - original draft. **Meichuan Liu:** Supervision, Funding acquisition, Conceptualization, Project administration, Resources, Writing - review & editing. **Huanhuan Sun:** Investigation, Formal analysis, Validation, Visualization. **Hanxing Lu:** Investigation, Formal analysis, Visualization. **Guohua Zhao:** Funding acquisition, Resources.

Acknowledgment

This work was financially supported by the National Natural Science Foundation of China (NSFC, Project Nos. 21777115, 21537003, 21377092), and the Science and Technology Commission of Shanghai Municipality (Project No. 14DZ2261100).

Appendix A. Supplementary data

Supplementary data to this article can be found online at https://doi.org/10.1016/j.bios.2019.111352.

References

Barchanska, H., Jodo, E., Price, R.G., Baranowska, I., Abuknesha, R., 2012. Chemosphere 87 (11), 1330–1334.
Bhardwaj, S.K., Bhardwaj, N., Mohanta, G.C., Kumar, P., Sharma, A.L., Kim, K.H., Deep, A., 2015. ACS Appl. Mater. Interfaces 7 (47), 26124–26130.
Buser, H.R., 1990. Environ. Sci. Technol. 24 (7), 1049–1058.
Chen, K., Liu, M.C., Zhao, G.H., Shi, H.J., Fan, L.F., Zhao, S.C., 2012. Environ. Sci. Technol. 46 (21), 11955–11961.
Eissa, S., Ng, A., Siaj, M., Zourob, M., 2014. Anal. Chem. 86 (15), 7551–7557.
Ellington, A.D., Szostak, J.W., 1990. Nature 346 (6287), 818–822.
Fu, C., Liu, C., Li, Y., Guo, Y., Luo, F., Wang, P., Guo, L., Qiu, B., Lin, Z., 2016. Anal. Chem. 88 (20), 10176–10182.
Ge, L., Wang, W., Hou, T., Li, F., 2016. Biosens. Bioelectron. 77, 220–226.
Guan, S.H., Huang, M.W., Li, X., Cai, Q., 2017. Anal. Lett. 51 (4), 613–625.
Gupta, V.K., Yola, M.L., Eren, T., Atar, N., 2015. Sensor. Actuator. B Chem. 218, 215–221.
Han, D.M., Jiang, L.Y., Tang, W.Y., Xu, J.J., Chen, H.Y., 2015. Electrochem. Commun. 51, 72–75.
Hou, T., Li, W., Liu, X., Li, F., 2015. Anal. Chem. 87 (22), 11368–11374.
Hou, T., Xu, N., Wang, W., Ge, L., Li, F., 2018. Anal. Chem. 90 (15), 9591–9597.
Hyer, K.E., Hornberger, G.M., Herman, J.S., 2001. J. Hydrol. 254 (1–4), 47–66.
Jiang, H., Adams, C., Graziano, N., Roberson, A., McGuire, M., Khiari, D., 2006. Environ. Eng. Sci. 23 (2), 357–366.
Joo, T.H., Kim, M.S., Kim, K., 1987. J. Raman Spectrosc. 18, 57–60.
Kubo, I., Shoji, R., Fuchiwaki, Y., Suzuki, H., 2008. Electrochemistry 76 (8), 541–544.
Lee, C.Y., Lee, K., Schmuki, P., 2013. Angew Chem. Int. Ed. Engl. 52 (7), 2077–2081.
Li, X., He, Y., Zhao, F., Zhang, W., Ye, Z., 2015. RSC Adv. 5 (70), 56534–56540.
Liu, M., Ke, H., Sun, C., Wang, G., Wang, Y., Zhao, G., 2019a. Talanta 194, 266–272.
Liu, M., Sun, C., Wang, G., Wang, Y., Lu, H., Shi, H., Zhao, G., 2019b. Electrochim. Acta 293, 220–229.
Liu, M., Ding, X., Yang, Q., Wang, Y., Zhao, G., Yang, N., 2017. J. Hazard Mater. 331, 309–320.
Liu, M., Yu, J., Ding, X., Zhao, G., 2016a. Electroanalysis 28 (1), 161–168.
Liu, G., Li, T., Yang, X., She, Y., Wang, M., Wang, J., Zhang, M., Wang, S., Jin, F., Jin, M., Shao, H., Jiang, Z., Yu, H., 2016b. Carbohydr. Polym. 137, 75–81.
Liu, S., Lin, Y., Wang, L., Liu, T., Cheng, C., Wei, W., Tang, B., 2014. Anal. Chem. 86 (8), 4008–4015.
Lu, B.J., Liu, M.C., Shi, H.J., Huang, X.F., Zhao, G.H., 2013. Electroanalysis 25 (3), 771–779.
Lu, C.H., Yang, H.H., Zhu, C.L., Chen, X., Chen, G.N., 2009. Angew Chem. Int. Ed. Engl. 121 (26), 4879–4881.
Madianos, L., Tsekenis, G., Skotadis, E., Patsiouras, L., Tsoukalas, D., 2018. Biosens. Bioelectron. 101, 268–274.
Osterloh, F.E., 2013. Chem. Soc. Rev. 42 (6), 2294–2320.

Pardieu, E., Cheap, H., Vedrine, C., Lazerges, M., Lattach, Y., Garnier, F., Remita, S., Pernelle, C., 2009. Anal. Chim. Acta 649 (2), 236–245.
Park, K.D., Raschke, M.B., Atkin, J.M., Lee, Y.H., Jeong, M.S., 2017. Adv. Mater. 29 (7), 1603601.
Peng, B., Tang, L., Zeng, G.G., Fang, S.Y., Ouyang, X.L., Long, B.Q., Zhou, Y.Y., Deng, Y.C., Liu, Y.N., Wang, J.J., 2018. Biosens. Bioelectron. 121, 19–26.
Qiao, Y., Li, J., Li, H., Fang, H., Fan, D., Wang, W., 2016. Biosens. Bioelectron. 86, 315–320.
Rubira, R.J.G., Camacho, S.A., Aoki, P.H.B., Maximino, M.D., Alessio, P., Martin, C.S., Oliveira Jr., O.N., Fatore, F.M., Paulovich, F.V., Constantino, C.J.L., 2014. Colloid Polym. Sci. 292 (11), 2811–2820.
Shi, H., Zhao, J., Wang, Y., Zhao, G., 2016. Biosens. Bioelectron. 81, 503–509.
Soejima, T., Maru, Y., Ito, S., 2013. B. Chem. Soc. JPN. 86 (9), 1065–1070.
Song, J., Wang, J., Wang, X., Zhao, W., Zhao, Y., Wu, S., Gao, Z., Yuan, J., Meng, C., 2016. Biosens. Bioelectron. 80, 614–620.
Sun, A.L., Zhang, Y.F., Sun, G.P., Wang, X.N., Tang, D., 2017. Biosens. Bioelectron. 89 (Pt 1), 659–665.
Tan, Y., Wei, X., Zhao, M., Qiu, B., Guo, L., Lin, Z., Yang, H.H., 2015. Anal. Chem. 87 (18), 9204–9208.
Wang, S., Zhao, S., Wei, X., Zhang, S., Liu, J., Dong, Y., 2017. Sensors 17 (3), 604.
Williams, R.M., Crihfield, C.L., Gattu, S., Holland, L.A., Sooter, L.J., 2014. Int. J. Mol. Sci. 15 (8), 14332–14347.
Wu, L., Li, F., Xu, Y., Zhang, J.W., Zhang, D., Li, G., Li, H., 2015. Appl. Catal. B Environ. 164 217-224.
Xuan, F., Luo, X., Hsing, I.M., 2012. Anal. Chem. 84 (12) 5216-5120.
Yan, G., Wang, Y., He, X., Wang, K., Liu, J., Du, Y., 2013. Biosens. Bioelectron. 44, 57–63.
Yu, Z.M., Zhao, G.H., Liu, M.C., Lei, Y.Z., Li, M.F., 2010. Environ. Sci. Technol. 44 (20), 7878–7883.
Zeng, R.J., Zhang, L.J., Su, L.S., Luo, Z.B., Zhou, Q., Tang, D.P., 2019. Biosens. Bioelectron. 133, 100–106.
Zhang, Z., Zhang, L., Hedhili, M.N., Zhang, H., Wang, P., 2013. Nano Lett. 13 (1), 14–20.
Zhao, L., Xu, H., Jiang, B., Huang, Y., 2017. Part. Part. Syst. Char. 34 (3), 1600323.
Zhao, W.,W., Xu, J.,J., Chen, H.,Y., 2015. Chem. Soc. Rev. 44 (15), 729–741.
Zhu, Y.H., Yan, K., Xu, Z.W., Wu, J.N., Zhang, J.D., 2019. Biosens. Bioelectron. 131, 79–87.